

# Stable periodic orbits for spacecraft around minor celestial bodies

Yu Jiang<sup>1,2</sup> (✉), Jürgen Arno Schmidt<sup>3</sup>, Hengnian Li<sup>1</sup>, Xiaodong Liu<sup>3</sup>, and Yue Yang<sup>4</sup>

1. State Key Laboratory of Astronautic Dynamics, Xi'an Satellite Control Center, Xi'an 710043, China

2. School of Aerospace Engineering, Tsinghua University, Beijing 100084, China

3. Astronomy Research Unit, University of Oulu, Finland

4. School of Software Engineering, Xi'an Jiaotong University, Xi'an 710049, China

## ABSTRACT

We are interested in stable periodic orbits for spacecraft in the gravitational field of minor celestial bodies. The stable periodic orbits around minor celestial bodies are useful not only for the mission design of the deep space exploration, but also for studying the long-time stability of small satellites in the large-size-ratio binary asteroids. The irregular shapes and gravitational fields of the minor celestial bodies are modeled by the polyhedral model. Using the topological classifications of periodic orbits and the grid search method, the stable periodic orbits can be calculated and the topological cases can be determined. Furthermore, we find five different types of stable periodic orbits around minor celestial bodies: (1) stable periodic orbits generated from the stable equilibrium points outside the minor celestial body; (2) stable periodic orbits continued from the unstable periodic orbits around the unstable equilibrium points; (3) retrograde and nearly circular periodic orbits with zero-inclination around minor celestial bodies; (4) resonance periodic orbits; (5) near-surface inclined periodic orbits. We take asteroids 243 Ida, 433 Eros, 6489 Golevka, 101955 Bennu, and the comet 1P/Halley for examples.

## KEYWORDS

asteroid  
comet  
deep space exploration  
periodic orbits  
stability  
orbit design

## Research Article

Received: 5 December 2016

Accepted: 29 July 2017

© 2017 Tsinghua University Press

## 1 Introduction

Missions to minor celestial bodies (here including asteroids and comets) and the discovery of large-size-ratio binary asteroids and triple asteroids make the study of stable periodic orbits around minor celestial bodies important [1–10]. Several previous studies investigated the periodic orbits around minor celestial bodies, such as Scheeres *et al.* [11], Elife and Lara [12], Palacián *et al.* [13], Vasilkova [14], Yu and Baoyin [15], Jiang *et al.* [16], Jiang and Baoyin [17], and Ni *et al.* [18].

Hamilton and Burns [19] studied the orbital stability zones around asteroid by assuming the asteroid to be a point mass and considering the solar radiation. Scheeres *et al.* [11] used the expansion of spherical harmonics method to model the gravitational field of 433 Eros and computed direct, nearly circular, equatorial periodic

orbits in the body-fixed frame of Eros. Elife and Lara [12] used a rotating straight segment to model the irregular shape of asteroid 433 Eros, and calculated periodic orbits around the segment. Vasilkova [14] used a triaxial ellipsoid to model the elongated asteroid and calculated several periodic orbits around equilibrium points of the triaxial ellipsoid. Palacián *et al.* [13] investigated the invariant manifold, periodic orbits, and quasi-periodic orbits around a rotating straight segment. Wang *et al.* [20] used the perturbation expansion with 2-order Legendre spherical harmonic coefficients to model the gravitational field of the asteroid and analyzed the stability of relative equilibrium of a spacecraft. Antoniadou and Voyatzis [21] studied the periodic orbits in the planetary system, and found that the stable periodic orbits will lead to long-term stability while the unstable orbits will lead to chaotic motion and destabilize the system.

✉ jiangyu\_xian.china@163.com

Scheeres *et al.* [22, 23] presented the dynamical equation, effective potential, and the Jacobian constant around the minor celestial bodies. Yu and Baoyin [15] gave a grid search method with the hierarchical parameterization to calculate the periodic orbits and periodic orbit families around minor celestial bodies. Jiang *et al.* [6] derived the linearised motion equations around equilibrium points and the characteristic equation of the equilibrium points of minor celestial bodies, which is useful to calculate the stability, topological classifications, and local motions around equilibrium points. The local periodic orbits and quasi-periodic orbits can be calculated by the analytic method presented from Jiang *et al.* [6]. The accuracy of analytic method is lower than that of the grid search method when computing the periodic orbits around equilibrium points [22, 24]. However, the compute speed of the analytic method is faster than that of the grid search method. If one wants to calculate the global periodic orbits, one can only use the numerical method, such as the grid search method [15, 16, 18]. The periodic orbit around a minor celestial body has six characteristic multipliers, at least two of which are equal to 1 [7, 15, 22].

Jiang *et al.* [7] found four kinds of bifurcations of periodic orbits when continuing the periodic orbits, including the real saddle bifurcations, the period-doubling bifurcations, the tangent bifurcations, and the Neimark–Sacker bifurcations. When continuing the periodic orbits around asteroids or comets, if the bifurcations occur, the stability of the periodic orbits may vary. Jiang and Baoyin [17] presented a conserved quantity which can restrict the number of periodic orbits on a fixed energy curved surface in the potential of a minor celestial body. They also discussed multiple bifurcations in the periodic orbit families around asteroids. Ni *et al.* [18] furthermore calculated several different kinds of multiple bifurcations in the periodic orbit families around asteroid 433 Eros.

Because bifurcations of stable periodic orbits may lead to unstable ones, when computing stable periodic orbits around minor celestial bodies, bifurcations are not expected to occur, especially for the design of stable periodic orbits for spacecrafts orbiting asteroids or comets, or for the study of stable periodic orbits for moonlets orbiting the primary in the binary or triple systems [3, 11, 19]. Jiang *et al.* [16] found a family of stable periodic orbits, which is retrograde, nearly circular, and with zero-inclinations relative to

the primary’s body-fixed frame. When continuing the periodic orbits, the characteristic multipliers collide at  $-1$  and pass through each other. The period-doubling bifurcation does not occur during the continuation. The four characteristic multipliers except two equal to 1 are in the unit circle. During the continuation, the characteristic multipliers will collide on the unit circle, but the Neimark–Sacker bifurcation does not occur. Using the contents about the continuity of periodic orbits during the change of parameters from Jiang *et al.* [7], we know that there exists a family of stable periodic orbits around each of the stable periodic orbit. Thus here we mainly discuss the stable periodic orbits around minor celestial bodies.

This paper is organized as follows. Section 2 focuses on the gravitational potential of minor celestial bodies. Section 3 discusses the monodromy matrix and characteristic multipliers of periodic orbits as well as the stability and topological classifications of stable periodic orbits. In Section 4, we find five different kinds of stable periodic orbits in the potential of minor celestial bodies. These different kinds of stable periodic orbits are found in the potential of several minor celestial bodies, including the comet 1P/Halley, the asteroids 243 Ida, 433 Eros, 6489 Golevka, and 101955 Bennu.

## 2 Gravitational potential

The shape and gravitational model of minor celestial bodies can be modeled by the polyhedral model [3, 25–27] or the hard/soft-sphere discrete element method [10, 28–30]. Asteroid 433 Eros is elongated, and has both concave and convex areas on surface. So we choose asteroid 433 Eros to calculate the irregular shape and effective potential. The physical and shape model of asteroid 433 Eros used here is generated by data from Gaskell [31] with the polyhedral model [25, 26]. The overall dimensions of asteroid 433 Eros are  $36 \text{ km} \times 15 \text{ km} \times 13 \text{ km}$  [32], the estimated bulk density is  $2.67 \text{ g} \cdot \text{m}^{-3}$  [32, 33], the rotational period is  $5.27025547 \text{ h}$  [32], and the moment of inertia is  $17.09 \times 71.79 \times 74.49 \text{ km}^2$  [33]. The modeling of 433 Eros employed 99,846 vertices and 196,608 faces [31]. Figure 1 shows the 3D shape of asteroid 433 Eros viewed from different directions. From Fig. 1, one can see that there are several craters with different size on the surface of asteroid 433 Eros. There is a large crater on the  $+y$  direction of the asteroid.

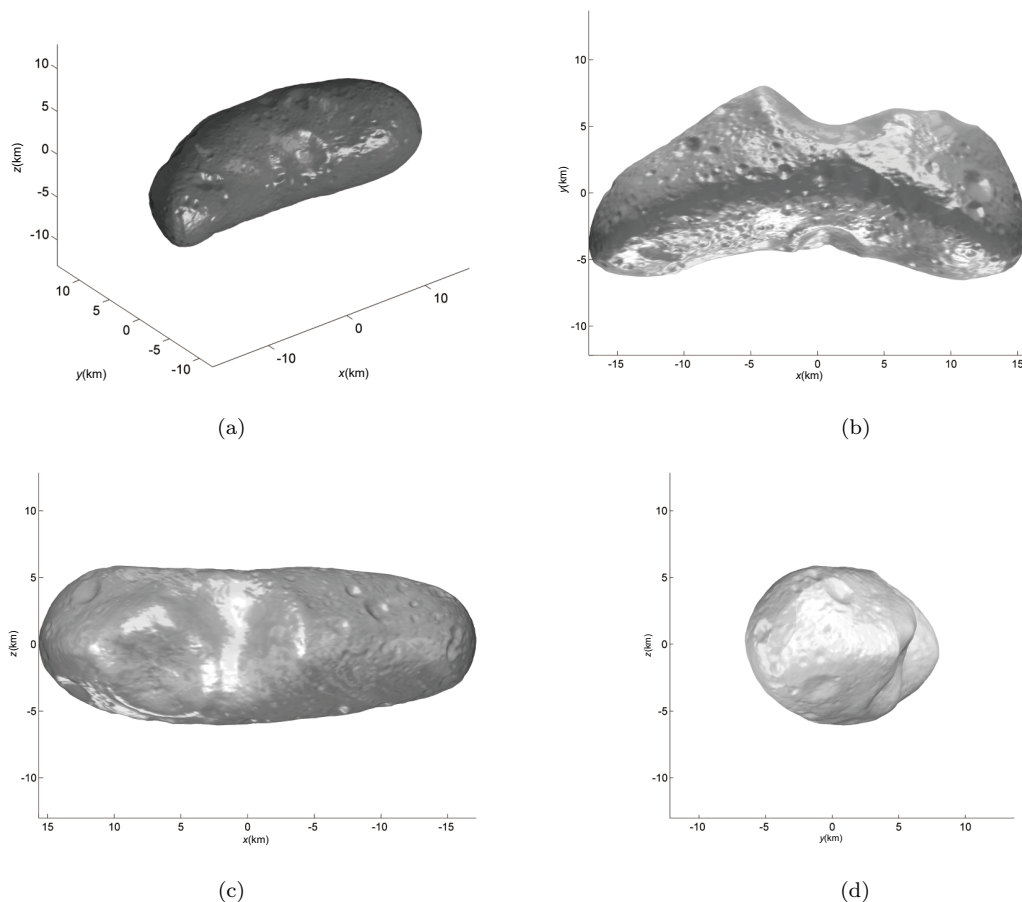


**Fig. 1** 3D shape of asteroid 433 Eros.

Figure 2 shows a 3D contour plot of the effective potential  $V$  for asteroid 433 Eros. The values for  $V$  are plotted in the  $xy$ ,  $yz$ , and  $zx$  planes. The structures of effective potential in the  $xy$ ,  $yz$ , and  $zx$  planes are quite different. More detailed contents to calculate the effective potential can be found in Jiang and Baoyin [17]. The positions of equilibrium points of asteroid 433 Eros is near the  $xy$  plane, but not in the  $xy$  plane, which implies that they are out-of-plane equilibrium points. More details about the equilibrium points of asteroids can be found in Chanut *et al.* [4], Jiang *et al.* [6], and Wang *et al.* [27].

### 3 Stable periodic orbits for spacecraft around asteroids and comets

#### 3.1 Monodromy matrix and characteristic multipliers

The dynamical equation of the spacecraft relative to

the body-fixed frame of the minor celestial body can be expressed in the symplectic form [7]:

$$\dot{z} = F(z) = J\nabla H(z) \tag{1}$$

where  $z = [ \mathbf{p} \ \mathbf{q} ]^T$ ,  $\mathbf{p} = (\dot{\mathbf{r}} + \boldsymbol{\omega} \times \mathbf{r})$  is the generalised momentum,  $\mathbf{q} = \mathbf{r}$  is the generalised coordinate,  $\mathbf{q}$  represents the position vector of the spacecraft relative to the body's body-fixed frame,  $J = \begin{pmatrix} \mathbf{0} & -\mathbf{I} \\ \mathbf{I} & \mathbf{0} \end{pmatrix}$ ,  $\mathbf{I}$  is a  $3 \times 3$  unit matrix,  $\mathbf{0}$  is a  $3 \times 3$  zero matrix,  $H = -\frac{\mathbf{p} \cdot \mathbf{p}}{2} + U(\mathbf{q}) + \mathbf{p} \cdot \dot{\mathbf{q}}$  is the Hamilton functions,  $U(\mathbf{q})$  represents the body's gravitational potential, and  $\nabla H(z) = \left( \frac{\partial H}{\partial \mathbf{p}} \ \frac{\partial H}{\partial \mathbf{q}} \right)^T$  is the gradient of  $H(z)$ .  $U(\mathbf{q})$  can be computed by the polyhedral model [26] with the shape data and physical parameters of the minor celestial body. The body-fixed frame is defined by the inertia axis, i.e.,  $x$ ,  $y$ , and  $z$  axes are the minimum, medium, and maximum inertia axis, respectively.

Denote  $S_p(T)$  as the set of periodic orbits with the

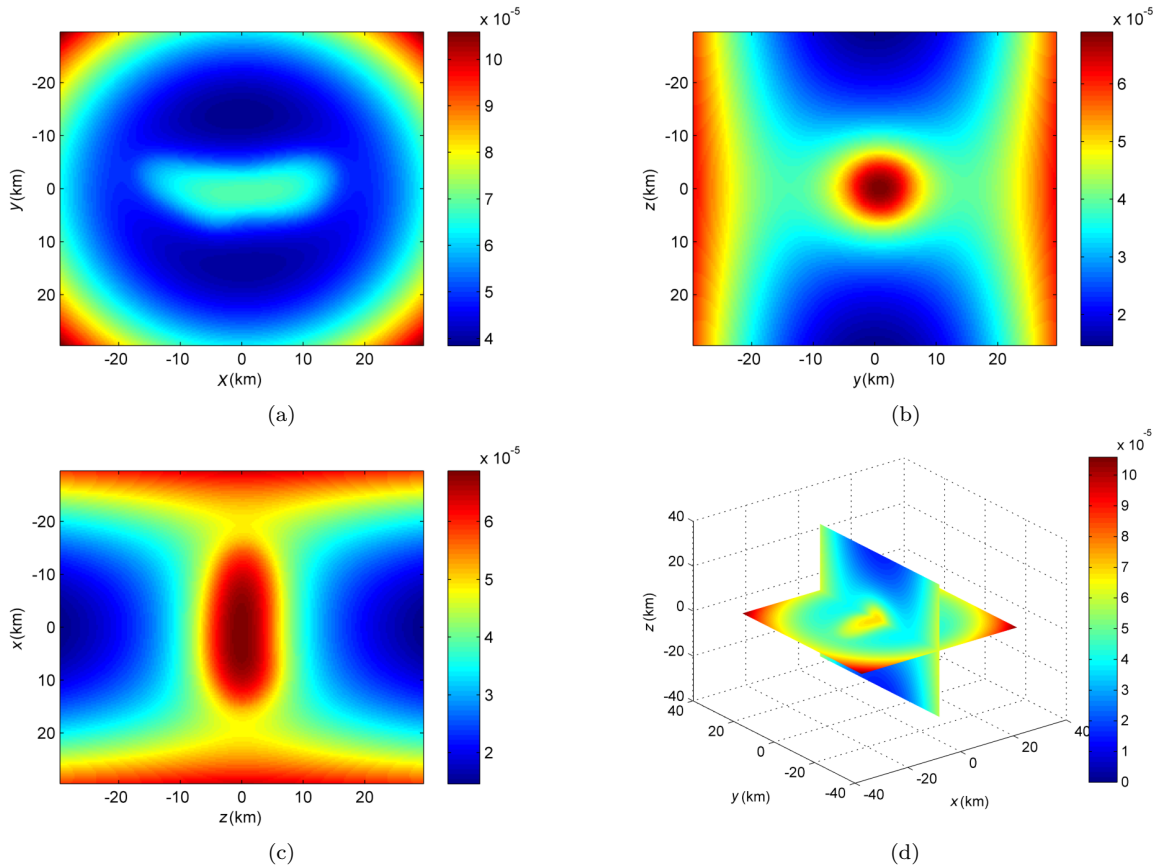


**Fig. 2** A 3D contour plot of the effective potential for 433 Eros (unit:  $\text{km}^2\cdot\text{s}^{-2}$ ).

period  $T$ . For each periodic orbit  $p \in S_p(T)$ , it has a  $6 \times 6$  matrix  $\nabla \mathbf{F} := \frac{\partial \mathbf{F}(\mathbf{z})}{\partial \mathbf{z}}$ , then the state transition matrix [7, 15, 21, 34] for the periodic orbit can be written as

$$\Phi(t) = \int_0^t \frac{\partial \mathbf{F}}{\partial \mathbf{z}}(p(\tau)) d\tau \quad (2)$$

the periodic orbit's monodromy matrix is then

$$\mathbf{M} = \Phi(T) \quad (3)$$

Characteristic multipliers of the periodic orbit are the eigenvalues of the monodromy matrix. Each periodic orbit has six characteristic multipliers, and all the characteristic multipliers take the form of  $e^{\pm\sigma \pm i\tau}$  ( $\sigma, \tau \in \mathbf{R}$ ;  $\sigma > 0$ ,  $\tau \in (0, \pi)$ ),  $\text{sgn}(\alpha)e^{\pm\alpha}$  ( $\alpha \in \mathbf{R}$ ,  $|\alpha| \in (0, 1)$ ),  $e^{\pm i\beta}$  ( $\beta \in (0, \pi)$ ),  $-1$ , and  $1$ , where  $\text{sgn}(\alpha) = \begin{cases} 1, & \alpha > 0 \\ -1, & \alpha < 0 \end{cases}$ .

### 3.2 Stability of periodic orbits

Distribution of six characteristic multipliers of the periodic orbit determines the topological classifications of periodic orbits [35]. The topological classifications of

stable periodic orbits [17] have 7 different cases, which are listed in Table 1.

More detailed contents of the topological classifications of periodic orbits can be seen in Jiang and Baoyin [17]. The topological case of the periodic orbits in the periodic orbit family may vary from the stable cases to the unstable cases. There are three bifurcations [7, 17, 18] related to the variety of the stability of the periodic orbits, i.e., Neimark–Sacker bifurcations, tangent bifurcations, as well as period-doubling bifurcations.

## 4 Different kinds of stable periodic orbits

In this section, we present five different kinds of stable periodic orbits around minor celestial bodies. These periodic orbits are calculated using the grid search method developed by Yu and Baoyin [15]. Before the periodic orbits are presented, we first give the length unit and time unit used here in Table 2. For instance, the first line in Table 2 means that the length unit

**Table 1** Topological classifications of stable periodic orbits

Topological case	Characteristic multiplier
Case N2 (non-degenerate cases)	$e^{\pm i\beta_j} (\beta_j \in (0, \pi); j = 1, 2   \beta_1 \neq \beta_2), \gamma_j (\gamma_j = 1; j = 1, 2)$
Case DP1 (degenerate periodic cases)	$e^{\pm i\beta_j} (\beta_j \in (0, \pi); j = 1), \gamma_j (\gamma_j = 1; j = 1, 2, 3, 4)$
Case DP2 (degenerate periodic cases)	$\gamma_j (\gamma_j = 1; j = 1, 2, 3, 4, 5, 6)$
Case K1 (Krein collision cases)	$e^{\pm i\beta_j} (\beta_j \in (0, \pi); j = 1, 2   \beta_1 = \beta_2), \gamma_j (\gamma_j = 1; j = 1, 2)$
Case PD1 (period-doubling cases)	$\gamma_j (\gamma_j = 1; j = 1, 2, 3, 4), \gamma_j (\gamma_j = -1; j = 1, 2)$
Case PD2 (period-doubling cases)	$\gamma_j (\gamma_j = 1; j = 1, 2), \gamma_j (\gamma_j = -1; j = 1, 2, 3, 4)$
Case PD3 (period-doubling cases)	$\gamma_j (\gamma_j = 1; j = 1, 2), \gamma_j (\gamma_j = -1; j = 1, 2), e^{\pm i\beta_j} (\beta_j \in (0, \pi); j = 1)$

**Table 2** Length unit and time unit used in this paper for minor bodies

Minor body	Length unit	Time unit
Comet 1P/Halley	15.140166 km	52.8 h
243 Ida	57.7917 km	4.63 h
433 Eros	34.4 km	5.2656 h
101955 Bennu	566.4413 m	4.288 h
6489 Golevka	685.15093 m	6.026 h

for motion around comet 1P/Halley is defined to be 15.140166 km, and the time unit is defined to be 52.8 h.

### 4.1 Generated from the stable equilibrium points

If the minor celestial bodies have stable equilibrium points outside the bodies, there exist three families of stable periodic orbits around each of the stable equilibrium points. There are several asteroids and comets having stable equilibrium points outside, including asteroids 4 Vesta [27], 2867 Steins [27], 6489 Golevka [6], 52760 [27], and comets 1P/Halley [9] as well as 9P/Tempel1 [27]. Jiang *et al.* [6] presented the analytic method to calculate the local periodic orbits around stable equilibrium points; however, the local periodic orbits calculated from the analytic method are not accurate enough. Using the grid search method developed by Yu and Baoyin [15], the stable periodic orbits around the stable equilibrium points can be calculated numerically. The grid search method has a high accuracy. The analytic method from Jiang *et al.* [6] can be used to give an initial estimate for the grid search method developed by Yu and Baoyin [15]. Jiang [24] applied the grid search method to the computation of the local periodic orbits around equilibrium points of asteroid 216 Kleopatra. Here we discuss the stable periodic orbits generated from the stable equilibrium points of minor celestial bodies. We

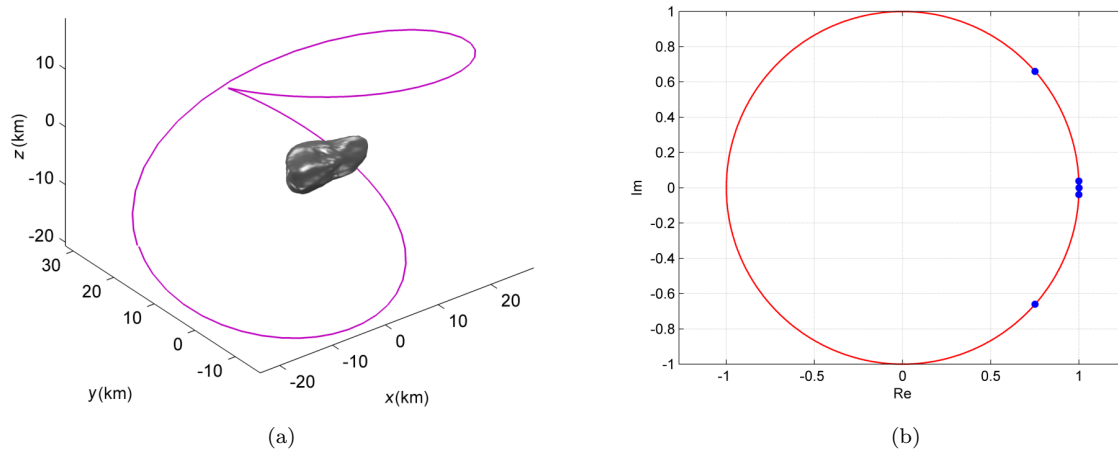
choose comet 1P/Halley to calculate the stable periodic orbits around the stable equilibrium points. We use the grid search method to search the periodic orbits and Eq. (3) to calculate the distribution of six characteristic multipliers of the periodic orbits. There are totally four equilibrium points outside the body of the comet 1P/Halley, two of them are stable, i.e., E2 and E4 [7, 27].

Figure 3 shows a periodic orbit continued from the stable equilibrium point E2 (the positions and serial numbers of equilibrium points in this paper can be seen in Wang *et al.* [27]) of the comet 1P/Halley. The period of this periodic orbit is 53.3971 h. The rotation period of the comet 1P/Halley is 52.8 h. Thus the ratio of the period of the periodic orbit relative to the period of the comet is 1.01130878575. From Fig. 3(b), one can see that the periodic orbit is stable.

Figure 4 shows a periodic orbit continued from the stable equilibrium point E4 of the comet 1P/Halley. The period of this periodic orbit is 53.3851 h. The ratio of the period of the periodic orbit and the period of the comet is 1.011080562545. From Fig. 4(b), one can see that the periodic orbit is stable. Table 3 presents the initial positions and the initial velocities of these two periodic orbits presented in Figs. 3 and 4, and the values are expressed in the body-fixed frame of 1P/Halley. In Table 3, periodic orbit 1 corresponds to the orbit presented in Fig. 3 while periodic orbit 2 corresponds to the orbit presented in Fig. 4.

### 4.2 Continued from the unstable periodic orbits around the unstable equilibrium points

The distribution of eigenvalues determines the topological cases of the equilibrium points around a uniformly rotating body. Jiang *et al.* [6] classified several different topological cases of the equilibrium points. From Jiang *et al.* [6] and Wang *et al.* [27],



**Fig. 3** A periodic orbit continued from the stable equilibrium point E2 of the comet 1P/Halley. The period is 53.3971 h, and the ratio of the period of the periodic orbit and the period of the comet is 1.01130878575. (a) 3D plot of the periodic orbit relative to the body-fixed frame of 1P/Halley; (b) distribution of six characteristic multipliers of the periodic orbit.

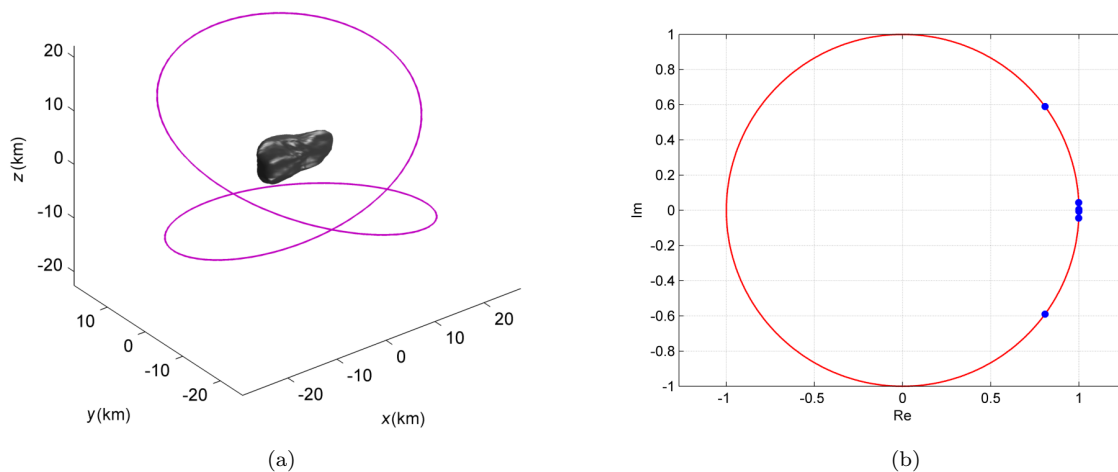


**Fig. 4** A periodic orbit continued from the stable equilibrium point E4 of the comet 1P/Halley. The period is 53.385053702375991 h, and the ratio of the period of the periodic orbit and the period of the comet is 1.011080562545. (a) 3D plot of the periodic orbit relative to the body-fixed frame of 1P/Halley; (b) distribution of six characteristic multipliers of the periodic orbit.

**Table 3** Initial positions and the initial velocities of periodic orbits in the body-fixed frame of 1P/Halley

Periodic orbit	Position	Velocity	Period
1	-1.43509739861	6.58815083642	1.01130878575
	1.10624686366	15.2096319563	
	-0.945745920199	4.79820012348	
2	1.44026951894	1.26316060312	1.011080562545
	-0.116377265356	-17.8320567684	
	-0.913778421911	3.71316717169	

we know that for most minor celestial bodies, if the external equilibrium points are unstable, they belong to Case 2 or Case 5, where Case 2 has the eigenvalues  $\pm\alpha_j$  ( $\alpha_j \in \mathbf{R}^+$ ;  $j = 1$ ) and  $\pm i\beta_j$  ( $\beta_j \in \mathbf{R}^+$ ;  $j = 1, 2$ ), while Case 5 has the eigenvalues  $\pm\sigma \pm i\tau$  ( $\sigma, \tau \in \mathbf{R}^+$ ) and  $\pm i\beta_j$  ( $\beta_j \in \mathbf{R}^+$ ;  $j = 1$ ). In the vicinity of the

equilibrium points which belong to Case 2, there exist two families of unstable periodic orbits. In the vicinity of the equilibrium points which belong to Case 5, there exists one family of unstable periodic orbits. When continuing these unstable periodic orbits, the amplitude of the periodic orbits increases gradually, and the periodic orbits become stable.

Here we choose the comet 1P/Halley and the primary of the binary asteroid 243 Ida to calculate the stable periodic orbits continued from the unstable periodic orbits around the unstable equilibrium points. Comet 1P/Halley has two unstable equilibrium points E1 and E3. The primary of the binary asteroid 243 Ida has four equilibrium points outside the body. All of them are unstable.

Figures 5 and 6 show two periodic orbits continued

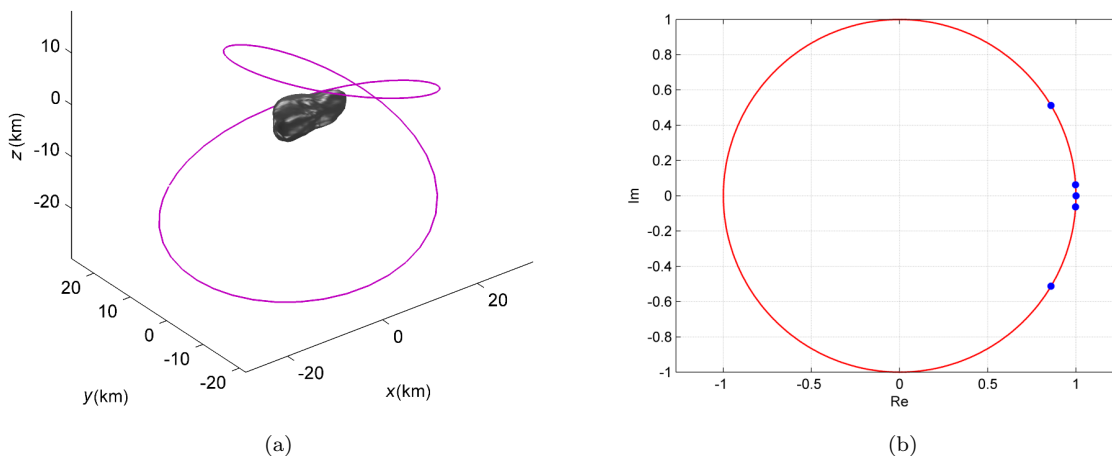


**Fig. 5** A periodic orbit continued from the stable equilibrium point E1 of the comet 1P/Halley. The period is 53.454 h, and the ratio of the period of the periodic orbit and the period of the comet is 1.01238521471. (a) 3D plot of the periodic orbit relative to the body-fixed frame of 1P/Halley; (b) distribution of six characteristic multipliers of the periodic orbit.

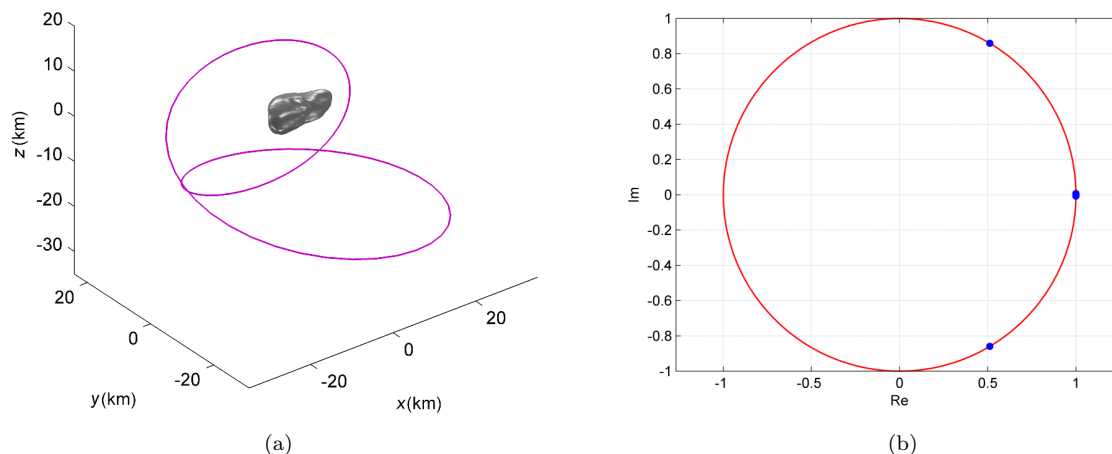


**Fig. 6** A periodic orbit continued from the stable equilibrium point E3 of the comet 1P/Halley. The period is 54.011925825 h, and the ratio of the period of the periodic orbit and the period of the comet is 1.02295314063. (a) 3D plot of the periodic orbit relative to the body-fixed frame of 1P/Halley; (b) distribution of six characteristic multipliers of the periodic orbit, there are four multipliers equal to 1.

from the unstable equilibrium points E1 and E3 of the comet 1P/Halley, respectively. The period of the periodic orbit presented in Fig. 5 is 53.454 h, and the ratio of the period of the periodic orbit and the period of the comet is 1.01238521471. The period of the periodic orbit presented in Fig. 6 is 54.0119 h, and the ratio of the period of the periodic orbit relative to the period of the comet is 1.02295314063. From Fig. 5(b) and Fig. 6(b), one can see that these two periodic orbits are stable.

Figures 7 and 8 show two periodic orbits continued from the unstable equilibrium points E2 and E4 of the primary of the binary asteroid 243 Ida, respectively. The period of the periodic orbit presented in Fig. 7 is 5.2447 h, and the ratio of the period of the periodic orbit and the period of the comet is 1.13276985098. The

periodic orbit presented in Fig. 7 is continued from the unstable equilibrium point E2, and it connects periodic orbit generated from equilibrium point E1. The period of the periodic orbit presented in Fig. 8 is 5.2678 h, and the ratio of the period of the periodic orbit and the period of the comet is 1.13775669387. From Fig. 7(b) and Fig. 8(b), one can see that these two periodic orbits are stable.

Table 4 presents the initial positions and the initial velocities of these four periodic orbits presented in Figs. 5–8, the values are expressed in the body-fixed frame of the minor bodies. In Table 4, periodic orbits 1 and 2 correspond to the orbits presented in Figs. 5 and 6, respectively; periodic orbits 3 and 4 correspond to the orbits presented in Figs. 7 and 8, respectively.

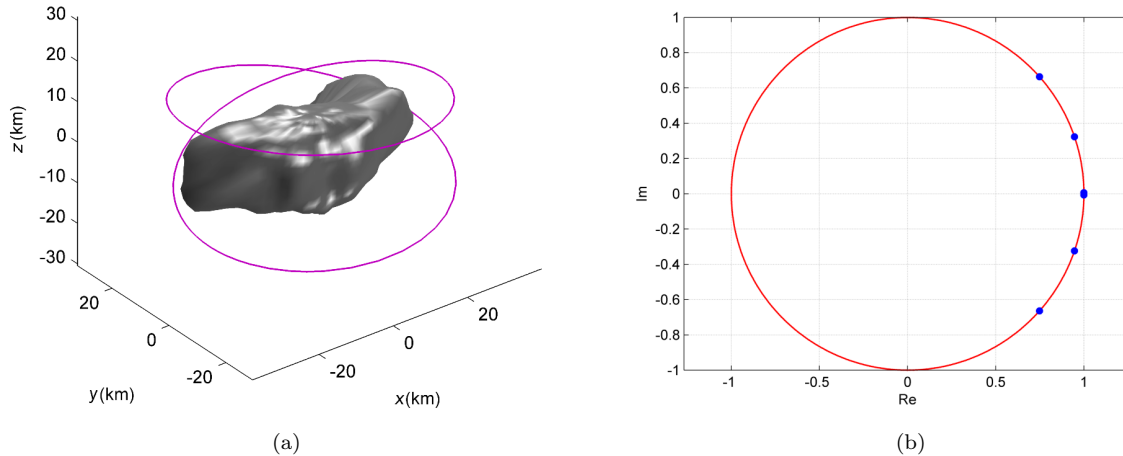


**Fig. 7** A periodic orbit continued from the stable equilibrium point E2 of the asteroid 243 Ida. The period is 5.244724410037399 h, and the ratio of the period of the periodic orbit and the period of the asteroid is 1.13276985098. (a) 3D plot of the periodic orbit relative to the body-fixed frame of 243 Ida; (b) distribution of six characteristic multipliers of the periodic orbit.

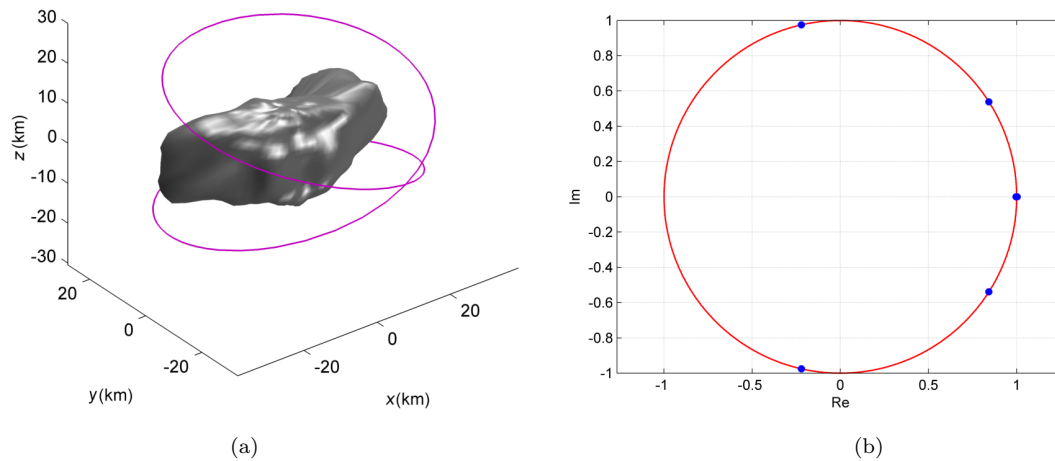


**Fig. 8** A periodic orbit continued from the stable equilibrium point E4 of the asteroid 243 Ida. The period is 5.2678134926181 h, and the ratio of the period of the periodic orbit and the period of the asteroid is 1.13775669387. (a) 3D plot of the periodic orbit relative to the body-fixed frame of 243 Ida; (b) distribution of six characteristic multipliers of the periodic orbit.

**Table 4** Initial positions and the initial velocities of periodic orbits in the body-fixed frame of 1P/Halley and 243 Ida

Periodic orbit	Position	Velocity	Period
1	-0.724053725841	14.3328568184	1.01238521471
	1.48667560655	8.78463438036	
	-1.33198379992	3.48528278685	
2	0.0508067344449	16.7180042361	1.02295314063
	1.58710718406	1.28433682355	
	-1.43117795230	-2.60834460269	
3	0.0626044457277	5.70149686669	1.13276985098
	0.532671731883	-0.332300886588	
	-0.0571937606260	1.49480516557	
4	0.365717153565	-3.96356504016	1.13775669387
	-0.376264464591	-3.96490101038	
	-0.100156740647	1.66824049654	

### 4.3 Retrograde and nearly circular periodic orbits with zero inclination

Jiang *et al.* [16] found a family of stable periodic orbits around the large-size-ratio triple asteroid 216 Kleopatra, which is nearly circular and retrograde with zero inclination. These periodic orbits are nearly circular and retrograde with zero inclination. The primary of 216 Kleopatra has seven equilibrium points, four of them are outside the body, and these four equilibrium points are all unstable. We choose some other minor celestial bodies with different structure of gravitational fields to calculate if similar orbits also exist. Asteroids 433 Eros, 101955 Bennu, and 6489 Golevka are taken for examples to calculate the periodic orbits. 433 Eros has totally five equilibrium points. Four of them are outside the body,

and all the external equilibrium points are unstable. 6489 Golevka also has totally five equilibrium points. Four of them are outside the body; however, two of the outside equilibrium points are unstable and other two outside equilibrium points are stable. 101955 Bennu has totally nine equilibrium points. These three asteroids have different structures of gravitational fields.

Figure 9 shows a family of periodic orbits around asteroid 433 Eros, and the periodic orbits are nearly circular and retrograde with zero inclination. The initial positions and velocities of these five periodic orbits in the periodic orbit family in the gravitational potential of 433 Eros are presented in Table 5. The vectors are expressed in the asteroid’s body-fixed frame. There are totally five periodic orbits plotted in Fig. 9. The period of the smallest periodic orbit is 7.0827 h with the ratio 1.345096. The period of the biggest periodic orbit is 7.6912 h with the ratio 1.460648. Here the ratio means

the ratio of the period of the periodic orbit relative to the period of the minor celestial body. From the inner to the outer, the periods of the periodic orbits become larger. This result is different from the period in the Kepler motion expressed in the inertial coordinate system. From Fig. 9(b), one can see that the orbits are not in the plane; they are curves in the normal direction.

Figure 10 shows another periodic orbit family around asteroid 433 Eros. The periodic orbits are also nearly circular and retrograde with zero inclination. The initial positions and velocities of these five periodic orbits in the gravitational potential of 433 Eros are presented in Table 6. The vectors are expressed in the asteroid’s body-fixed frame. There are totally seven periodic orbits plotted in Fig. 9. The periodic orbits are stable. Figures 10(c) and 10(d) present the distribution of six characteristic multipliers of the smallest and biggest periodic orbits among the seven periodic orbits

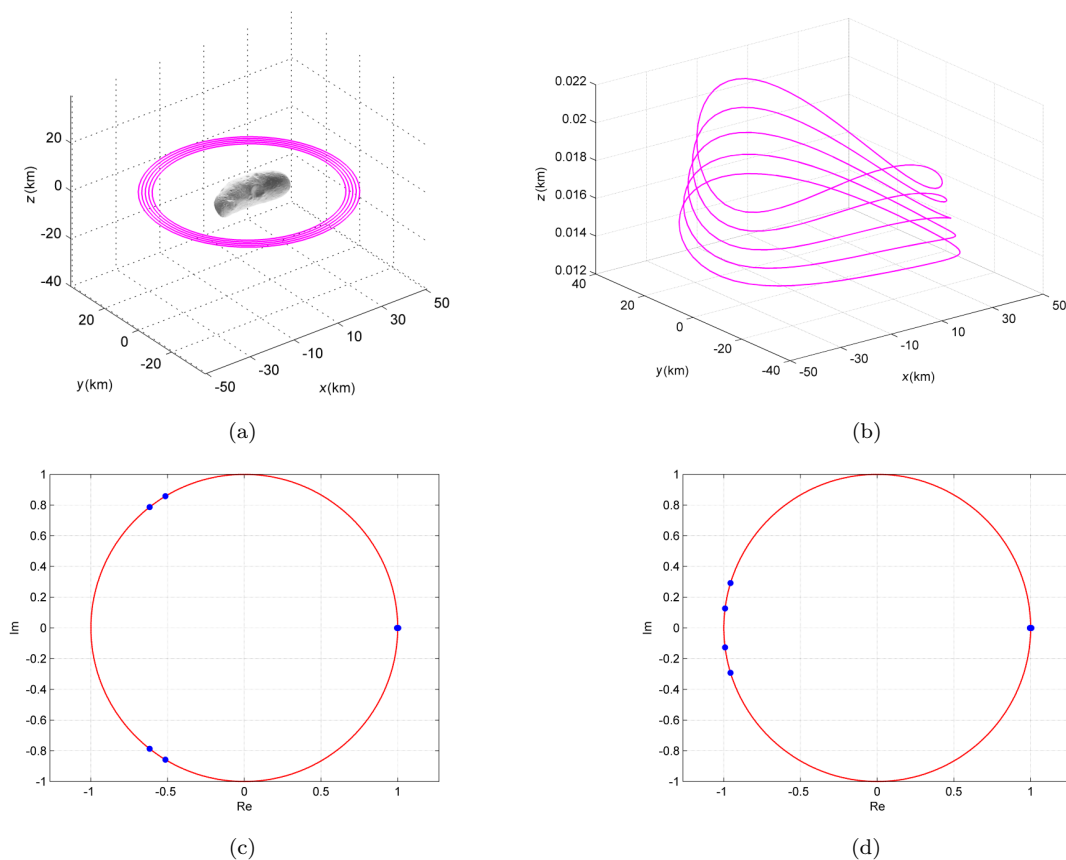


**Fig. 9** A family of nearly circular periodic orbits around asteroid 433 Eros which are retrograde with zero inclination. (a) 3D plot of the periodic orbits relative to the body-fixed frame of 433 Eros. Five periodic orbits are plotted; from the inner to the outer, the periods of the periodic orbits become bigger. (b) 3D plot of the periodic orbits (without the asteroid) relative to the body-fixed frame of 433 Eros. (c) Distribution of six characteristic multipliers of the periodic orbit (the smallest periodic orbit among the five periodic orbits plotted). The period is 7.0827 h, and the ratio of the period of the periodic orbit and the period of the asteroid is 1.345096. (d) Distribution of six characteristic multipliers of the periodic orbit (the biggest periodic orbit among the five periodic orbits plotted). The period is 7.6912 h, and the ratio of the period of the periodic orbit and the period of the asteroid is 1.460648.

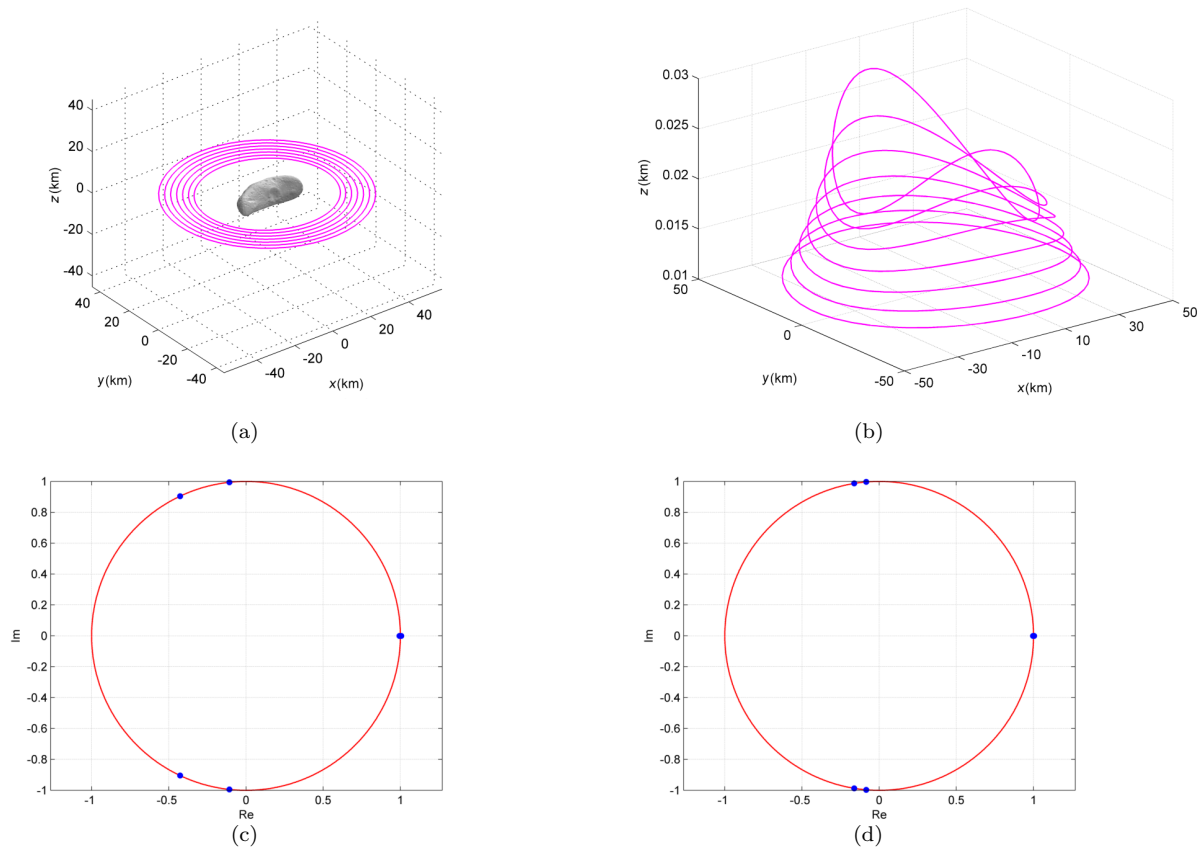


**Fig. 10** A family of nearly circular periodic orbits around asteroid 433 Eros which are retrograde with zero inclination. (a) 3D plot of the periodic orbits relative to the body-fixed frame of 433 Eros. Seven periodic orbits are plotted; from the inner to the outer, the periods of the periodic orbits become smaller. (b) 3D plot of the periodic orbits (without the asteroid) relative to the body-fixed frame of 433 Eros. (c) Distribution of six characteristic multipliers of the periodic orbit (the smallest periodic orbit among the seven periodic orbits plotted). The period is 8.656684 h, and the ratio of the period of the periodic orbit and the period of the asteroid is 1.64400724599. (d) Distribution of six characteristic multipliers of the periodic orbit (the biggest periodic orbit among the seven periodic orbits plotted). The period is 6.684357 h, and the ratio of the period of the periodic orbit and the period of the asteroid is 1.26943881082.

plotted. From Figs. 10(c) and 10(d), one can see that the characteristic multipliers on the unit circle move during the continuation.

The period of the smallest periodic orbit is 8.656684 h with the ratio 1.64400724599. The period of the biggest periodic orbit is 6.684357 h with the ratio 1.26943881082. From the inner to the outer, the periods of the periodic orbits become smaller. This result is different from the above results presented in Fig. 9 and Table 5. Thus the periodic orbit family presented in Fig. 10 is different from the periodic orbit family presented in Fig. 9. We can conclude that there are at least two periodic orbit families in the potential of one minor celestial body, which are nearly circular, retrograde, and stable with zero inclination.

For the asteroid 101955 Benu, the rotation period is 4.288 h. For the asteroid 6489 Golevka, the rotation period is 6.026 h.

Figure 11 shows a periodic orbit around asteroid

101955 Benu, and Fig. 12 shows a periodic orbit around asteroid 6489 Golevka. Both of the two periodic orbits are nearly circular, stable, and retrograde with zero inclination. The initial positions and velocities of these two periodic orbits in the periodic orbit family in the gravitational potential of the asteroids are presented in Table 7. Furthermore, the periodic orbit presented in Fig. 12 has the period ratio 0.495486995181, which is near the 1:2 resonance of the period of the periodic orbit and the rotation period of the asteroid 6489 Golevka. Jiang *et al.* [16] found periodic orbits in the potential of asteroid 216 Kleopatra; the periodic orbits are nearly circular retrograde and stable with zero inclination; the asteroid 216 Kleopatra has seven equilibrium points. From Figs. 9–12, one can see that the periodic orbits which are nearly circular, retrograde, and stable with zero inclination exist not only on the gravitational field of asteroid 216 Kleopatra, but also in the gravitational field of 433 Eros, 101955 Benu, and 6489 Golevka.

**Table 5** Initial positions and the initial velocities of periodic orbits in the body-fixed frame of 433 Eros (indexes 1 to 5 mean the orbits from inner to outer)

Periodic orbit	Position	Velocity	Period
1	0.743990716373	-4.19745020860	1.34509555159
	-0.894842961577	-3.44719333572	
	0.000419947168	0.000221072321	
2	0.683634268907	-4.12698424359	1.36878554932
	-0.895480402681	-3.10294685101	
	0.000448414280	0.000263961275	
3	0.614417150401	-4.06181001461	1.39553123024
	-0.899312199598	-2.72236601436	
	0.000480602904	0.000314113036	
4	0.595998913791	-3.83587690126	1.42591950706
	-0.866964082507	-2.57348128953	
	0.000511515830	0.000387281366	
5	0.547342936704	-3.68645740335	1.46064834302
	-0.854052941398	-2.28916792332	
	0.000547689132	0.000473375432	

**Table 6** Initial positions and the initial velocities of periodic orbits in the body-fixed frame of 433 Eros (indexes 1 to 7 mean the orbits from inner to outer)

Periodic orbit	Position	Velocity	Period
1	0.226020373236	3.05135726080	1.64400724599
	0.831549571341	-0.755105170473	
	0.000815731943	-0.000787043149240	
2	0.162260294966	3.69842543490	1.53615360513
	0.925373223566	-0.620219330154	
	0.000698149394	-0.000317281286244	
3	0.118572781769	4.31126220291	1.45298231634
	1.01015364846	-0.494283666047	
	0.000592999780	-0.000142173246285	
4	0.039313088475	4.90077984986	1.38965306382
	1.09256772994	-0.174726400201	
	0.000508929461	-0.0462158783466	
5	0.0877117956974	5.43432437124	1.34047716511
	1.16503659385	-0.405607013915	
	0.00044077741409	-0.0000433255175181	
6	-0.0194496986212	5.97936660822	1.30132599619
	1.24241338092	0.0923344130837	
	0.000386702840792	-0.00000568727917105	
7	-0.01819579281	6.50081649913	1.26943881082
	1.31630038108	0.0889931429895	
	0.000342011597241	-0.00000361670859952	

This implies that the periodic orbits which are nearly circular retrograde and stable with zero inclination may widely exist in the potential of different gravitational field structure of minor celestial bodies.

### 4.4 Resonance

In this section, resonant periodic orbit means that the ratio of the period of the periodic orbit relative to the period of the asteroid is an integer. Russell

**Table 7** Initial positions and the initial velocities of periodic orbits in the body-fixed frame of 101955 Bennu and 6489 Golevka (periodic orbit 1 is the orbit around 101955 Bennu and periodic orbit 2 is the orbit around 6489 Golevka)

Periodic orbit	Position	Velocity	Period
1	0.671591383153	-2.01971118787	1.96251392508
	-0.586009389218	-2.60968398375	
	-0.0631586635050	-0.0536311486152	
2	-0.802329098318	0.927694676293	0.495486995181
	0.0683264606186	10.1907427252	
	-0.00221645697675	0.0258563463006	

[36] presented a 17:21 periodic orbit around asteroid 4 Vesta and several trajectories around highly irregular asteroid 4179 Toutatis. Jiang *et al.* [16] presented 4 resonant periodic orbits around asteroid 101955 Bennu, and one of them is stable. 101955 Bennu is the only one minor celestial body which has the maximum number of equilibrium points in the current study. There are totally 9 equilibrium points in the potential of asteroid 101955 Bennu, and 8 of them are outside the body.

Here we find resonant periodic orbits around other minor celestial bodies, including asteroid 243 Ida and 6489 Golevka. The length unit and time unit for motion around 243 Ida are the same as that in Section 4.2. The length unit and time unit for motion around 6489 Golevka are the same as that in Section 4.3.

Figure 13 presents a resonant periodic orbit around the primary of the binary asteroid 243 Ida. From Fig. 13(b), one can see that the periodic orbit is stable, and has four characteristic multipliers equal to 1. The initial positions and velocities of the periodic orbit in the gravitational potential of 243 Ida are presented in Table 8. The vectors are expressed in the asteroid’s body-fixed frame. The periodic orbit is calculated using the Poincaré section; it has 8 intersections with the Poincaré section.

Figures 14 and 15 present two 2:1 resonant periodic orbits around the asteroid 6489 Golevka. From Figs. 14(b) and 15(b), one can see that these two periodic orbits are stable. The periodic orbit presented in Fig. 14 has two characteristic multipliers equal to 1, while the periodic orbit presented in Fig. 15 has four characteristic multipliers equal to 1. The initial positions and velocities of the periodic orbits in the periodic orbit family in the gravitational potential of 6489 Golevka are presented in Table 8. The vectors are expressed in the asteroid’s body-fixed frame. These two periodic orbits are calculated using the Poincaré section; both of them have 3 intersections with the Poincaré section.

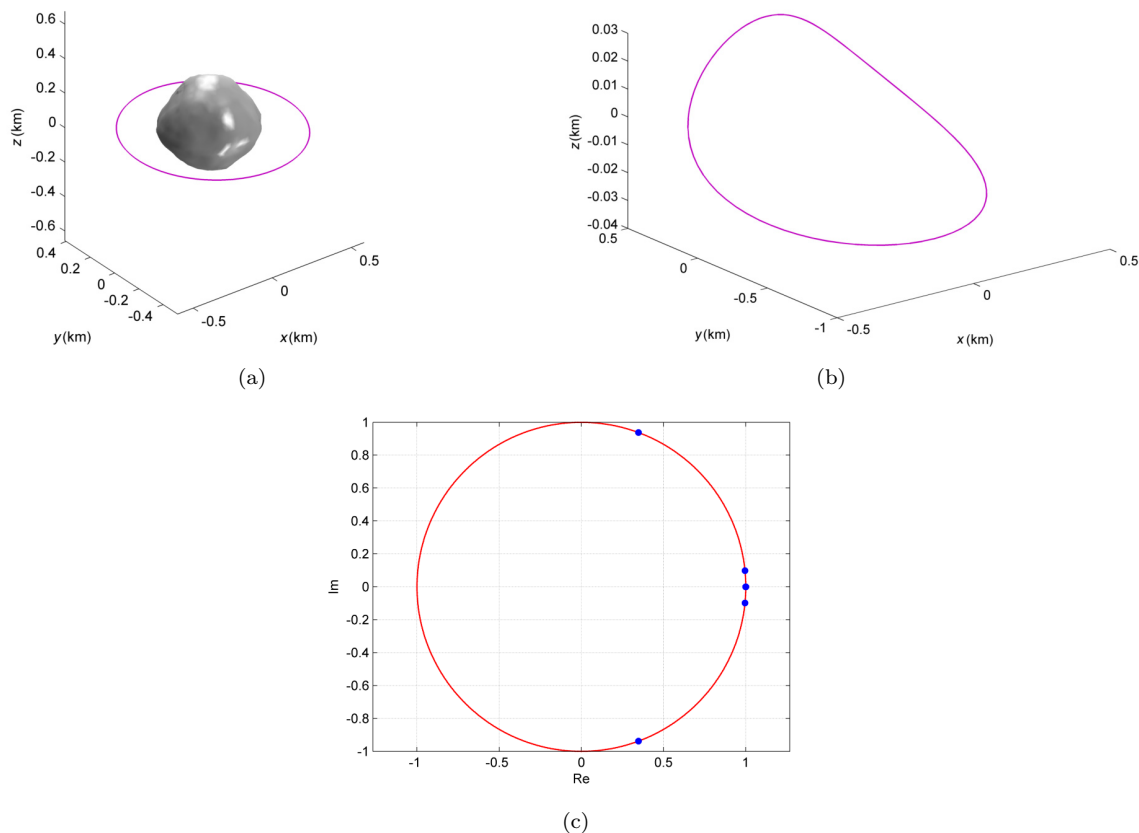


**Fig. 11** A nearly circular periodic orbit around asteroid 101955 Benu which is retrograde with zero inclination. The period is 8.41525971074304 h, and the ratio of the period of the periodic orbit and the period of the comet is 1.96251392508. (a) 3D plot of the periodic orbit relative to the body-fixed frame of 101955 Benu; (b) 3D plot of the periodic orbit relative to the body-fixed frame of 101955 Benu (without the asteroid); (c) distribution of six characteristic multipliers of the periodic orbit.

#### 4.5 Near-surface inclined periodic orbits

The length unit and time unit for motion around the comet 1P/Halley are the same as that in Section 4.1. Figure 16 shows two different near-surface inclined periodic orbits, and these periodic orbits are non-resonant. From Fig. 16(b), one can see that these two periodic orbits are really inclined relative to the  $xy$  plane (i.e., the equatorial plane of the comet). From Fig. 16, one can also see that these two periodic orbits are near the surface of the body and stable. The initial positions and velocities of these two periodic orbits in the gravitational potential of 1P/Halley are presented in Table 9. The vectors are expressed in the comet's body-fixed frame. It is a remarkable fact that the ratio of the period of these two periodic orbits and the rotation period is smaller than 0.2.

#### 4.6 Discussion of different kinds of stable periodic orbits

From the above sections, we know that there exist

several different kinds of stable periodic orbits around an irregular-shaped celestial body.

(1) **Generated from the stable equilibrium points.** If the asteroid has stable equilibrium points outside the body, then there exist three families of stable periodic orbits around each of the stable equilibrium points [6, 24]. During the continuation, the periodic orbit families will change from stable to unstable (see Fig. 17 for instance).

(2) **Continued from the unstable periodic orbits around the unstable equilibrium points.** If the asteroid has no stable equilibrium points outside the body, then there exists one family of unstable periodic orbits around the unstable equilibrium point if the topological classifications of the equilibrium point belong to Case 5 [6]; for Case 2 of the unstable equilibrium point, there exist two family of unstable periodic orbits around the equilibrium point. These unstable periodic orbits can be continued until the periodic orbits become stable.

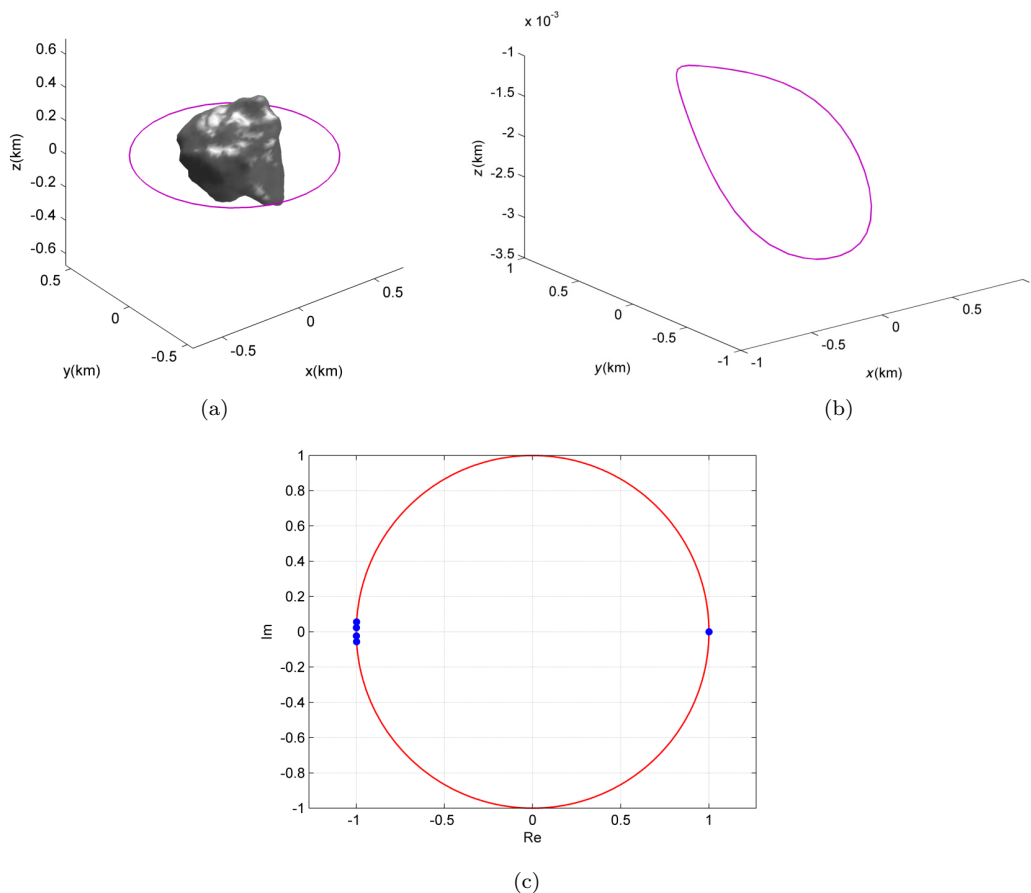


**Fig. 12** A nearly circular periodic orbit around asteroid 6489 Golevka which is retrograde with zero inclination. The period is 2.985804632960706 h, and the ratio of the period of the periodic orbit and the period of the asteroid is 0.495486995181. (a) 3D plot of the periodic orbit relative to the body-fixed frame of 6489 Golevka; (b) 3D plot of the periodic orbit relative to the body-fixed frame of 6489 Golevka (without the asteroid); (c) distribution of six characteristic multipliers of the periodic orbit.

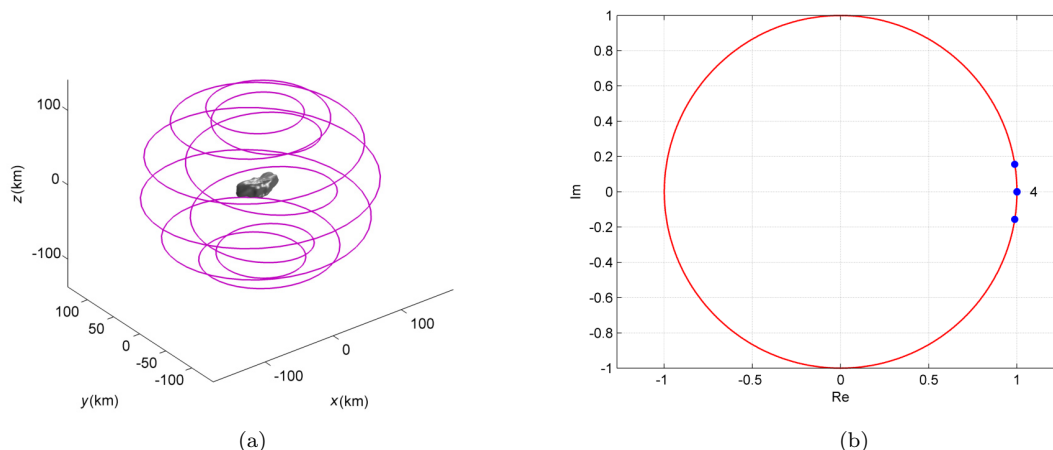


**Fig. 13** A resonant periodic orbit around asteroid 243 Ida. The ratio of the period of the periodic orbit and the period of the comet is 9.00525500454. (a) 3D plot of the periodic orbit relative to the body-fixed frame of 243 Ida; (b) distribution of six characteristic multipliers of the periodic orbit.

(3) **Retrograde and nearly circular periodic orbits with zero inclination.** There exist periodic orbit families which are nearly circular, and retrograde relative to the body-fixed frame of the asteroid [16, 18].

In addition, the inclinations of the periodic orbits relative to the asteroid’s body-fixed frame are nearly equal to zero.

(4) **Resonance.** There exist several resonant periodic

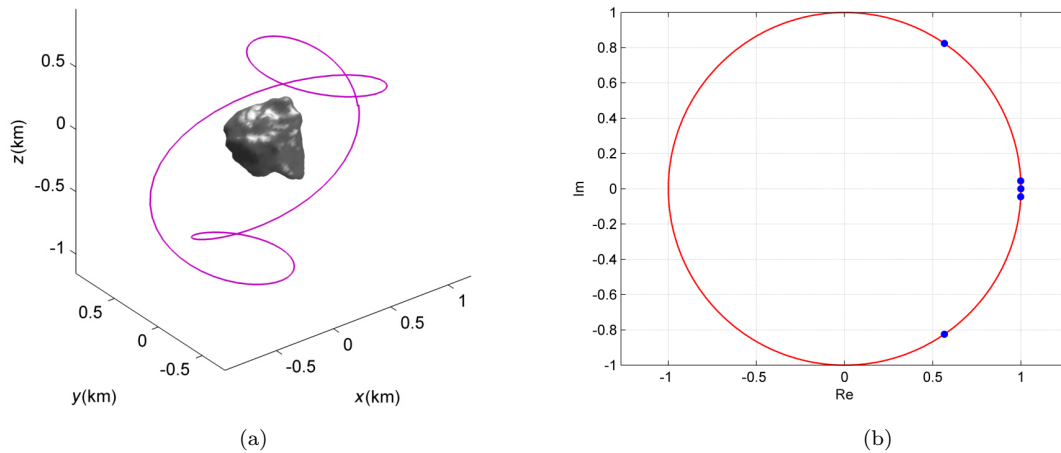


**Fig. 14** A resonant periodic orbit around asteroid 6489 Golevka. The ratio of the period of the periodic orbit and the period of the comet is 2.00558121907. (a) 3D plot of the periodic orbit relative to the body-fixed frame of 6489 Golevka; (b) distribution of six characteristic multipliers of the periodic orbit.

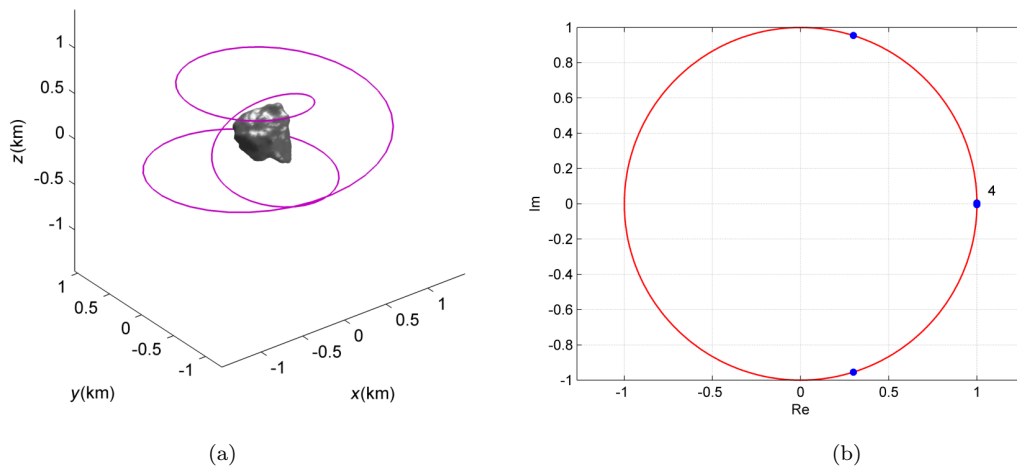


**Fig. 15** A resonant periodic orbit around asteroid 6489 Golevka. The ratio of the period of the periodic orbit and the period of the comet is 2.01369508451. (a) 3D plot of the periodic orbit relative to the body-fixed frame of 6489 Golevka; (b) distribution of six characteristic multipliers of the periodic orbit.

orbit families which are stable [16].

(5) **Near-surface inclined periodic orbits.** There exist several near-surface inclined periodic orbits around the asteroid, for which the distance between the periodic orbit and the mass center of the asteroid is smaller than the distance between the outside equilibrium point and the mass center of the asteroid.

Among these five different kinds of stable periodic orbits, (1) has been found in Jiang *et al.* [6], and (3) and (4) can be found in Jiang *et al.* [16]. (2) and (5) are found for the first time in this paper. However, the previous studies did not study and classify different kinds of stable periodic orbits around minor celestial bodies. During the continuation of retrograde nearly circular, and stable periodic orbits with zero inclination around minor bodies, our results imply that the periodic

orbits with the above characteristics can be found in the potential of different gravitational field structure of minor celestial bodies. In addition, there may be at least two periodic orbit families around one minor celestial body. Both of them are retrograde and nearly circular, and stable with zero inclination.

For the two near-surface inclined periodic orbits, it is notable that the ratio of the period of these two periodic orbits relative the rotation period is smaller than 0.2, which may be useful for us to search more kinds of near-surface inclined periodic orbits around other minor celestial bodies.

## 5 Conclusions

We analyze the stable periodic motions of spacecraft in

**Table 8** Initial positions and the initial velocities of periodic orbits in the body-fixed frame of 243 Ida and 6489 Golevka (periodic orbits 1, 2, and 3 are the initial values plotted in Figs. 13, 14, and 15, respectively. Periodic orbit 1 is around 243 Ida, periodic orbits 2 and 3 are around 6489 Golevka)

Periodic orbit	Position	Velocity	Period	Resonant ratio
1	0.897672329355	-8.73659445212	9.00525500454	9:1
	-1.29090224639	-6.14694020168		
	-0.0477816158615	1.55083729969		
2	0.616839318105	-3.66314369527	2.00558121907	2:1
	-0.719651400484	-6.19748150670		
	0.535816234907	-3.96827654611		
3	0.470335130163	6.89848549170	2.01369508451	2:1
	0.555139854298	-6.28441207004		
	0.164844445024	4.07158633235		

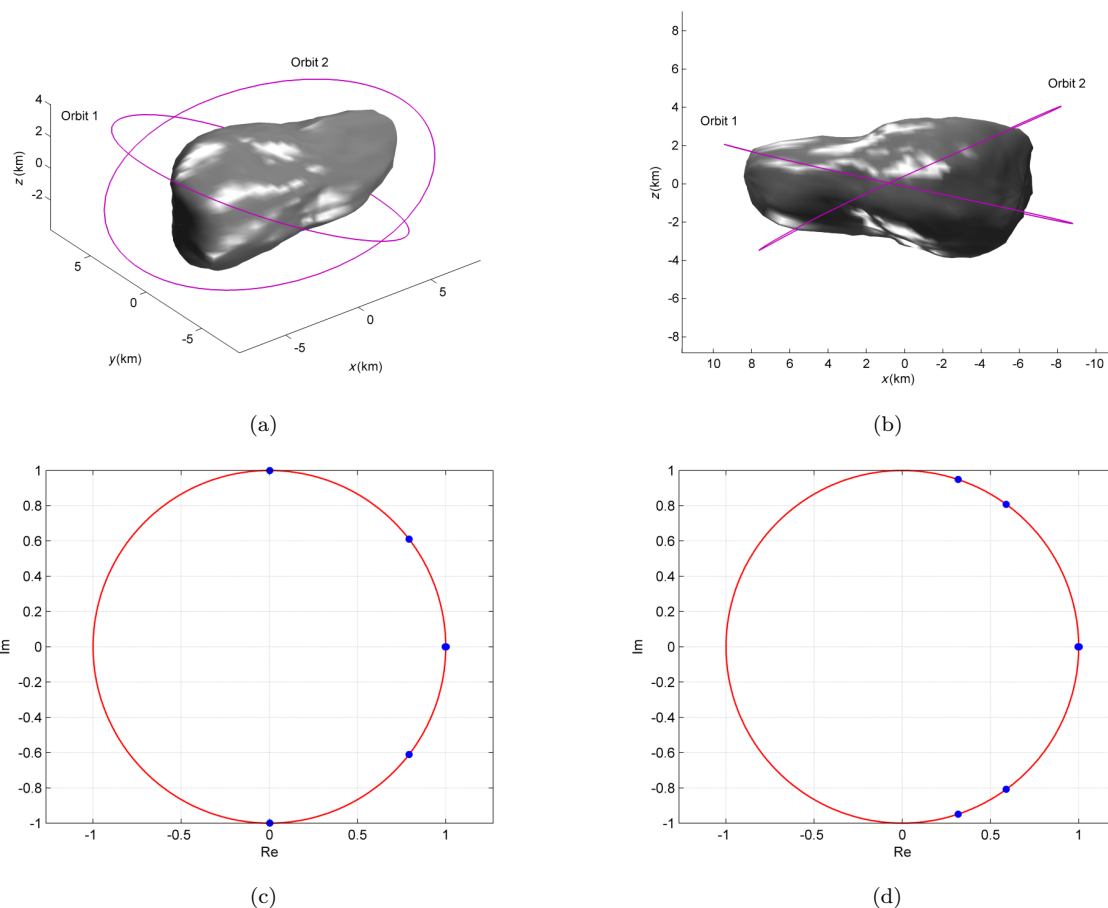


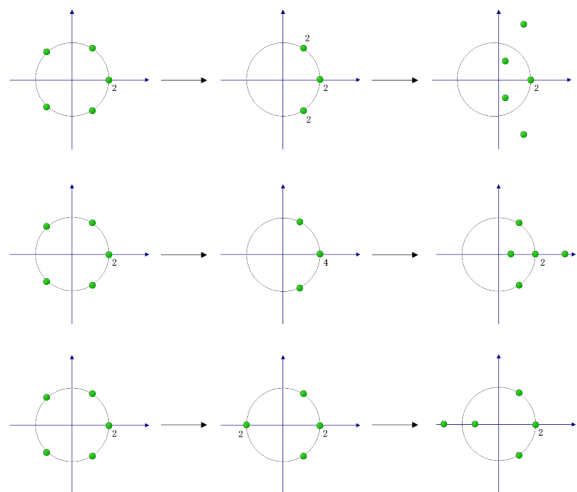
**Fig. 16** Two near-surface inclined periodic orbits around comet 1P/Halley. (a) 3D plot of the periodic orbits relative to the body-fixed frame of 1P/Halley; (b) periodic orbit relative to the body-fixed frame of 1P/Halley, viewed from +y axis; (c) distribution of six characteristic multipliers of the periodic orbit 1; (d) distribution of six characteristic multipliers of the periodic orbit 2.

the gravitational field of minor celestial bodies. The grid search method is used to calculate the periodic orbits. We use the shapes, positions, inclinations, retrograde or not, topological classifications, continuation properties, section planes, as well as the resonance ratios to analyze the different kinds of stable periodic motions around

asteroids and comets. Five kinds of stable periodic orbits are classified: (1) stable periodic orbits generated from the stable equilibrium points outside the minor celestial body; (2) stable periodic orbits continued from the unstable periodic orbits around the unstable equilibrium points; (3) periodic orbits which are retrograde and

**Table 9** Initial positions and the initial velocities of periodic orbits in the body-fixed frame of 1P/Halley

Periodic orbit	Position	Velocity	Period
1	0.0629890965760	-19.6763270413	0.180282795026
	-0.587664950749	-1.40740002652	
	0.00132142402742	-4.43845099506	
2	-0.229339377692	16.6681557777	0.174110986925
	0.517590660887	7.95258808390	
	0.128585669518	-7.27379326767	

**Fig. 17** Examples of the stability variety of periodic orbit families generated from the stable equilibrium points.

nearly circular with zero inclination; (4) resonant periodic orbits; (5) near-surface inclined stable periodic orbits.

Minor celestial bodies with different structure of gravitational fields are taken to calculate these stable periodic orbits, including asteroid 243 Ida, 433 Eros, 6489 Golevka, 101955 Bennu, and the comet 1P/Halley. The results of the stable periodic orbits around minor celestial bodies are useful for the mission design of the deep space exploration and the study of the configurations and stabilities of small satellites in the large-size-ratio binary asteroids.

## Acknowledgements

This research was supported by the State Key Laboratory of Astronautic Dynamics Foundation (No. 2016ADL0202).

## References

[1] Scheeres, D. J., Fahnestock, E. G., Ostro, S. J., Margot,

- J.-L., Benner, L. A. M., Broschart, S. B., Bellerose, J., Giorgini, J. D., Nolan, M. C., Magri, C., Pravec, P., Scheirich, P., Rose, R., Jurgens, R. F., De Jong, E. M., Suzuki, S. Dynamical configuration of binary near-Earth asteroid (66391) 1999 KW4. *Science*, **2006**, 314(5803): 1280–1283.
- [2] Taylor, P. A., Margot, J. L. Binary asteroid systems: Tidal end states and estimates of material properties. *Icarus*, **2011**, 212(2): 661–676.
- [3] Chanut, T. G. G., Winter, O. C., Tsuchida, M. 3D stability orbits close to 433 Eros using an effective polyhedral model method. *Monthly Notices of the Royal Astronomical Society*, **2014**, 438(3): 2672–2682.
- [4] Chanut, T. G. G., Winter, O. C., Amarante, A., Araújo, N. C. S. 3D plausible orbital stability close to asteroid (216) Kleopatra. *Monthly Notices of the Royal Astronomical Society*, **2015**, 452(2): 1316–1327.
- [5] Chanut, T. G. G., Aljbaae, S., Carruba, V. Mascon gravitation model using a shaped polyhedral source. *Monthly Notices of the Royal Astronomical Society*, **2015**, 450(4): 3742–3749.
- [6] Jiang, Y., Baoyin, H., Li, J., Li, H. Orbits and manifolds near the equilibrium points around a rotating asteroid. *Astrophysics and Space Science*, **2014**, 349(1): 83–106.
- [7] Jiang, Y., Yu, Y., Baoyin, H. Topological classifications and bifurcations of periodic orbits in the potential field of highly irregular-shaped celestial bodies. *Nonlinear Dynamics*, **2015**, 81(1–2): 119–140.
- [8] Jiang, Y., Baoyin, H., Li, H. Collision and annihilation of relative equilibrium points around asteroids with a changing parameter. *Monthly Notices of the Royal Astronomical Society*, **2015**, 452(4): 3924–3931.
- [9] Jiang, Y., Baoyin, H., Wang, X., Yu, Y., Li, H., Peng, C., Zhang, Z. Order and chaos near equilibrium points in the potential of rotating highly irregular-shaped celestial bodies. *Nonlinear Dynamics*, **2016**, 83(1–2): 231–252.
- [10] Jiang, Y., Zhang, Y., Baoyin, H. Surface motion relative to the irregular celestial bodies. *Planetary and Space Science*, **2016**, 127: 33–43.
- [11] Scheeres, D. J., Williams, B. G., Miller, J. K. Evaluation of the dynamic environment of an asteroid: Applications to 433 Eros. *Journal of Guidance, Control, and Dynamics*, **2000**, 23(3): 466–475.
- [12] Elipe, A., Lara, M. A simple model for the chaotic motion around (433) Eros. *The Journal of the Astronautical Sciences*, **2003**, 51(4): 391–404.
- [13] Palacian, J. F., Yanguas, P., Gutiérrez-Romero, S. Approximating the invariant sets of a finite straight segment near its collinear equilibria. *SIAM Journal of Applied Dynamical Systems*, **2006**, 5(1): 12–29.
- [14] Vasilkova, O. Three-dimensional periodic motion in the vicinity of the equilibrium points of an asteroid. *Astronomy & Astrophysics*, **2005**, 430(2): 713–723.
- [15] Yu, Y., Baoyin, H. Generating families of 3D periodic

- orbits about asteroids. *Monthly Notices of the Royal Astronomical Society*, **2012**, 427(1): 872–881.
- [16] Jiang, Y., Baoyin, H., Li, H. Periodic motion near the surface of asteroids. *Astrophysics and Space Science*, **2015**, 360(2): 63.
- [17] Jiang, Y., Baoyin, H. Periodic orbit families in the gravitational field of irregular-shaped bodies. *The Astronomical Journal*, **2016**, 152(5): 137.
- [18] Ni, Y., Jiang, Y., Baoyin, H. Multiple bifurcations in the periodic orbit around Eros. *Astrophysics and Space Science*, **2016**, 361(5): 170.
- [19] Hamilton, D. P., Burns, J. A. Orbital stability zones about asteroids: II. The destabilizing effects of eccentric orbits and of Solar radiation. *Icarus*, **1992**, 96(1): 43–64.
- [20] Wang, Y., Xu, S., Zhu, M. Stability of relative equilibria of the full spacecraft dynamics around an asteroid with orbit–attitude coupling. *Advances in Space Research*, **2014**, 53(7): 1092–1107.
- [21] Antoniadou, K. I., Voyatzis, G. Resonant periodic orbits in the exoplanetary systems. *Astrophysics and Space Science*, **2014**, 349(2): 657–676.
- [22] Scheeres, D. J., Ostro, S. J., Hudson, R. S., Werner, R. A. Orbits close to asteroid 4769 Castalia. *Icarus*, **1996**, 121(1): 67–87.
- [23] Scheeres, D. J., Ostro, S. J., Hudson, R. S., De Jong, E. M., Suzuki, S. Dynamics of orbits close to asteroid 4179 Toutatis. *Icarus*, **1998**, 132(1): 53–79.
- [24] Jiang, Y. Equilibrium points and periodic orbits in the vicinity of asteroids with an application to 216 Kleopatra. *Earth, Moon and Planets*, **2015**, 115(1–4): 31–44.
- [25] Werner, R. A. The gravitational potential of a homogeneous polyhedron or don't cut corners. *Celestial Mechanics and Dynamical Astronomy*, **1994**, 59(3): 253–278.
- [26] Werner, R. A., Scheeres, D. J. Exterior gravitation of a polyhedron derived and compared with harmonic and mascon gravitation representations of asteroid 4769 Castalia. *Celestial Mechanics and Dynamical Astronomy*, **1997**, 65(3): 313–344.
- [27] Wang, X., Jiang, Y., Gong, S. Analysis of the potential field and equilibrium points of irregular-shaped minor celestial bodies. *Astrophysics and Space Science*, **2014**, 353(1): 105–121.
- [28] Richardson, D. C., Michel, P., Walsh, K. J., Flynn, K. W. Numerical simulations of asteroids modelled as gravitational aggregates with cohesion. *Planetary and Space Science*, **2009**, 57(2): 183–192.
- [29] Hirabayashi, M., Scheeres, D. J. Analysis of asteroid (216) Kleopatra using dynamical and structural constraints. *The Astrophysical Journal*, **2014**, 780(2): 160.
- [30] Gabriel, T. S. J., Scheeres, D. J. Energy dissipation end states of the sphere restricted planar three-body problem with collisional interaction. *Monthly Notices of the Royal Astronomical Society*, **2016**, 463(1): 794–801.
- [31] Gaskell, R. W. Gaskell Eros Shape Model V1.0. NEAR-A-MSI-5-EROSHAPE-V1.0. NASA Planetary Data System. **2008**.
- [32] Petit, A., Souchay, J., Lhotka, C. High precision model of precession and nutation of the asteroids (1) Ceres, (4) Vesta, (433) Eros, (2867) Steins, and (25143) Itokawa. *Astronomy & Astrophysics*, **2014**, 565: A79.
- [33] Miller, J. K., Konopliv, A. S., Antreasian, P. G., Bordi, J. J., Chesley, S., Helfrich, C. E., Owen, W. M., Wang, T. C., Williams, B. G., Yeomans, D. K., Scheeres, D. J. Determination of shape, gravity, and rotational state of asteroid 433 Eros. *Icarus*, **2002**, 155(1): 3–17.
- [34] Scheeres, D. J. Orbital mechanics about small bodies. *Acta Astronautica*, **2012**, 72: 1–14.
- [35] Tresaco, E., Elife, A., Riaguas, A. Computation of families of periodic orbits and bifurcations around a massive annulus. *Astrophysics and Space Science*, **2012**, 338(1): 23–33.
- [36] Russell, R. P. Survey of spacecraft trajectory design in strongly perturbed environments. *Journal of Guidance, Control, and Dynamics*, **2012**, 35(3): 705–720.



**Yu Jiang** received his bachelor degree from Peking University, and master degree as well as Ph.D. degree from Tsinghua University. He is now a researcher in State Key Laboratory of Astronautic Dynamics and Tsinghua University. His research interests are in the dynamics and control around multiple asteroid systems, surface motion and soft-landing on minor bodies, space debris, as well as cometary dust dynamics. E-mail: jiangyu\_xian\_china@163.com.



**Jürgen Arno Schmidt** received his diploma degree in theoretical physics from the University of Saarbrücken, Germany, and his Ph.D. degree in theoretical physics from the University of Potsdam, Germany. He is now professor in the Astronomy Research Unit of the University of Oulu, Finland. His research interests in the field of celestial mechanics focus on the dynamics of circumplanetary dust and dense planetary rings. He is co-investigator in the science teams of the Cassini Cosmic Dust Analyzer, the Surface Dust Mass Analyzer of the Europa Clipper Mission, and the JANUS camera onboard the Jupiter Icy Moons Explorer. E-mail: jrschmid@sun3.oulu.fi.



**Hengnian Li** received his bachelor degree in mathematical computation from Lanzhou University, and master degree in computer science from National University of Defence Technology as well as Ph.D. degree in system science and engineering from Xi'an Jiaotong University. He is now the director as

well as a researcher in State Key Laboratory of Astronautic Dynamics, China. His research interests cover many fields in spacecraft dynamics and control, including to orbital perturbation models, orbital tracking and precision determination, artificial intelligent machine learning, etc. E-mail: Henry\_xsc@Aliyun.com.



**Xiaodong Liu** received his B.S. degree in engineering mechanics from Shandong University in 2008, and Ph.D. degree in aeronautical and astronautical science and technology from Tsinghua University in 2013. He received the grand prize for graduate students at Tsinghua University, and national

excellent doctor thesis in the field of aeronautical and astronautical science and technology. Currently he is a postdoctoral researcher in the Astronomy Research Unit at University of Oulu, Finland. His research interest focuses on circumplanetary and interplanetary dust dynamics, tenuous planetary rings, estimate of dust hazard to spacecraft, and orbital dynamics around non-spherical bodies. E-mail: xiaodong.liu@oulu.fi.



**Yue Yang** received her bachelor degree from Sichuan University. She is now a graduate student in Xi'an Jiaotong University, majoring in software engineering. Her research interests are in data mining and performance abnormality diagnosis. E-mail: yang\_yue2015@stu.xjtu.edu.cn.